American Journal of Engineering Research (AJER)
e-ISSN: 2320-0847 p-ISSN : 2320-0936
Volume-5, Issue-11, pp-23-30
www.ajer.org
Research Paper Open Access

Numerical Analysis of Switching and Current-Voltage Characteristics of Graphene Nano-Ribbon Field Effect Transistors

Farhan-Bin-Tarik[†1] and Rawdah Mahmood[2]
[1]*Department of Electrical & Computer Engineering, Clemson University, SC, USA*
[2]*Department of Electrical & Electronic Engineering, University of Dhaka, Bangladesh*

ABSTRACT: *Graphene is one of the recently discovered materials from which graphene nano-ribbon (acronym, GNR) is derived. GNR has a great impact on the nano scale field effect transistors (FET) which has been tried to demonstrate in this study. Here, we have illustrated an analytical model of GNRFET for spatial distributions of the electric potential along the channel. The analysis is performed to find out the dependences of the source-drain current on the drain voltages as well as on the back gate and top gate voltages for different geometric parameters of the device. The switching on and switching off characteristics have been demonstrated in terms of current density, channel length and gate-voltage.*
Keywords: *GNRFET, Gate Voltage, Energy Bandgap, Channel Length, Current Density, Potential Distribution*

I. INTRODUCTION

It has not been many a year since graphene was discovered. Graphene is, basically, a carbon-based purely two dimensional material with large amount of captivating properties, especially, the prospect of ultrahigh carrier mobilities beyond those of the conventional semiconductors [1], [2], [3]. The fascinating prospects of graphene have aggravated rigorous work focused on the intensification of graphene metal-oxide-semiconductor field-effect transistors (MOSFETs) [4], [5].

Nano-ribbons (also called nano-graphene ribbons or nano-graphite ribbons), often abbreviated GNRs, are strips of graphene with ultra-thin width (<50 nm). Graphene ribbons were introduced as a theoretical model by Mitsutaka Fujita and co-authors to examine the edge and nano-scale size effect in graphene [6], [7], [8].Ifgraphene is narrowed into slender graphene nano-ribbon (GNRs), a sizeable band gapopens[9], [10].

A large number of applications of GNRFET have maneuvered the advantages of GNR such as nano switch [11], tunneling transistor [12] etc in the recent times. GNRFET has powerful ability to control the electrostatics and hence is expected to reduce the short channel effect [13], which depends on the device electrostatics. Pei et al. [14] exploited an analytical modeling of the current at ballistic limit to evaluate GNRFET. Thiele et al. [15] applied a quasi-analytical modeling approach to analyze the current-voltage characteristics.

In this paper, we have tried to study the current density of GNRFET varying the carrier density in the device. An analytical GNRFET model [16] has been used for numerical simulation. The equations of the model include Poisson's equation in the weak non-locality approximation. Room temperature (300K) has been considered for electrical measurement. The source-drain current density versus drain voltage dependencies have been exhibited for different gate-voltages. The condition for ON-OFF with the current-voltage characteristics have been demonstrated.

II. THEORETICAL ANALYSIS

2.1 Device Structure

As the name suggests, GNRFET is field effect transistor (FET) with graphene nano-ribbon (GNR) as the channel material. In this experiment, we have used GNRFET common source circuit for simulation and hence examined the DC characteristics. Different gate geometries have been applied to investigate the effect of gate geometry on GNRFET performance. The analytical model has been used to calculate the potential distributions in the GNR-FET as a function of the back gate, top gate, and drain voltages, V_b, V_g, and V_d respectively. We consider GNRFET with n-type channel. Therefore, positive back gate voltage, i.e., $V_b>0$ and

negative top gate voltage, i.e., $V_g<0$ have been assumed. Schematic of the device structure is shown in Fig.1 and Fig.2 (a), (b) show the side view and top view of the device respectively.

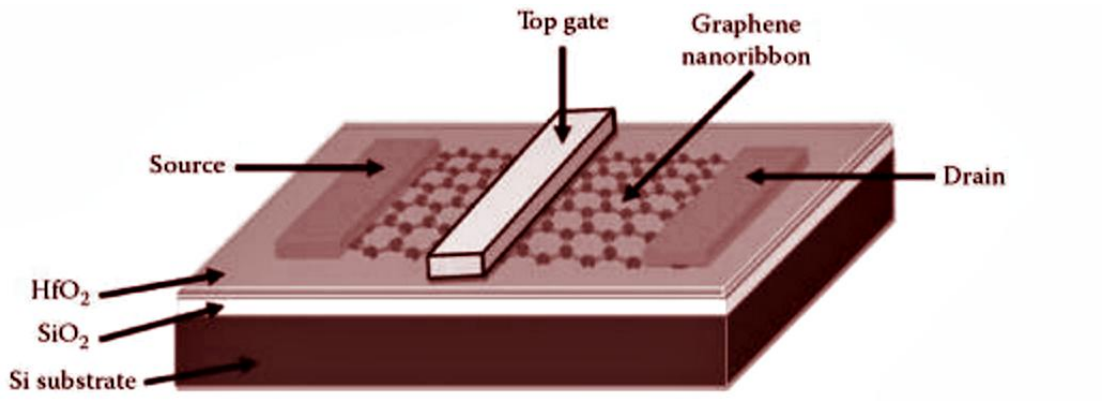

Fig.1: Structure of a GNRFET with GNR as the channel material [17].

2.2 The Analytical Model of GNRFET

The energy spectrum of Graphene strips (nano-ribbons) with a gap between the valence and conduction bands mainly depends on the nano-ribbon width d:

$$\varepsilon_{p,n}^{-1} = \pm v\sqrt{(p^2 + \left(\frac{\pi\hbar}{d}\right)^2 n^2)} \qquad (1)$$

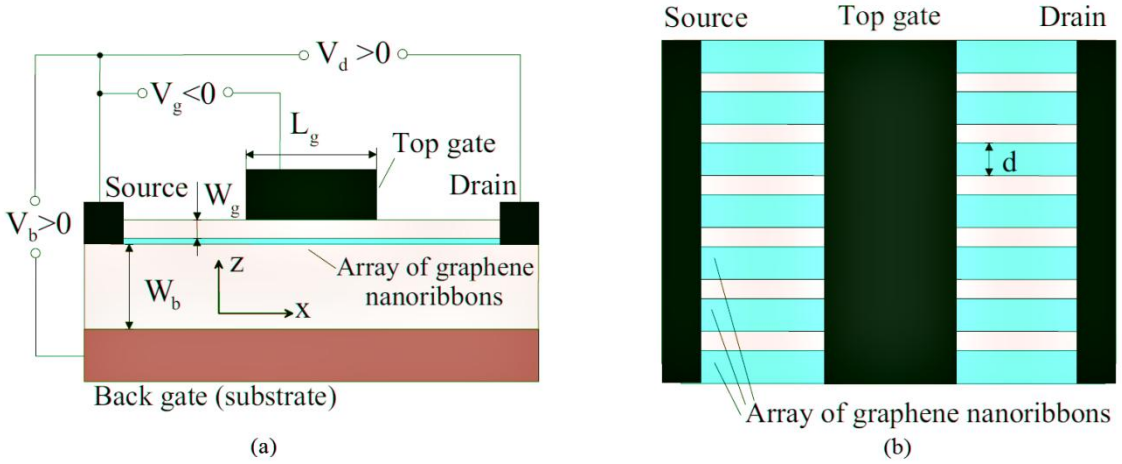

Fig.2: (a) Side view of GNRFET structure,(b) Top view of GNRFET structure [16]

Here, v= 108cms^{-1} is the characteristic velocity of the electron and hole spectra, P is the momentum in along the nano-ribbon, ħ is the reduced Planck constant, and n = 1, 2, 3, … is the sub and index.

The appearance of the band gap between the valence and conduction bands and specifically the density of states (DOS) as a function of the energy is the issue of the quantization corresponding to eqn. (1) of the electron and hole energy spectra in nano-ribbons since the electron and hole are confined in one of the lateral directions. The electron (hole) gas become degenerated at fairly high back gate voltages in relatively narrow nano-ribbons with quantized energy spectrum and the pertinent energy gap between the sub ands in the valence and conduction band which is exactly opposite to grapheme with zero energy gap. In this paper we have regulated the model such that the GNR-FET operates under the condition that the electron gas in the channel is non-degenerate. Hence, the back gate voltage is considered to be reasonably high in order to keep the electron density moderated, the electron gas in the channel non-degenerated and also for the electrons to occupy only the lowest (n = 1) sub and in the conduction band nano-ribbons. The highly conducting channel sections adjacent to the source and drain are equipotential. The potentials are equal to the potentials of the source and drain contacts, i.e., equal to ø = 0 and ø = V_d, respectively. The GNR-FET region under the top gate (the device active region) defined as follows: $L_g \leq x \leq L_g/2$, $W_b \leq z \leq W_g$, where L_g is the length of the top gate, and W_b and W_g are the thicknesses of the layers between graphene and the back and top gates, respectively. The following equation is used to find the potential distribution along the channel,

$$\frac{W_b+W_g}{3}\frac{\partial^2\phi}{\partial x^2}-\frac{\phi-V_b}{W_b}-\frac{\phi-V_g}{W_g}=\frac{4\pi e}{\varepsilon}(\Sigma_- -\Sigma_+) \qquad (2)$$

with the boundary conditions,

$$\phi|_x = -L_g/2 = 0, \qquad \phi|_x = -L_g/2 = V_d \qquad (3)$$

Here, Σ_- and Σ_+ are the electron and hole sheet densities in the channel, e is the electron charge, and is the dielectric constant of the material separating the channel from the gates. Eqn. (2), which governs the electric potential, $\phi = \phi(x) = \psi(x, 0)$, in the channel is a consequence of the two-dimensional Poisson equation for the electric potential $\psi = \psi(x, z)$ for the active region under consideration in the weak non-locality approximation [16], [18] this equation provides solutions, which can be obtained from the exact solution of the two-dimensional Poisson by the expansion in powers of the parameter $W_b^3 + W_g^3/45(W_b + W_g)L^2$, which is much smaller than unity in the situation under consideration. The relationship between the potential in the channel and the electron and hole charge becomes limited by neglecting the first term in the left-hand side of eqn. (2) where the lowest approximation in such an expansion corresponding to the so-called gradual channel approximation proposed by W. Shockley. Thus, eqn. (2) can be used when $\delta < 1$ and, hence, when $L \geq \max(W_b, W_g)$. In particular, it is possible to study essentially non-uniform potential distributions in the GNR-FET channel and the short-gate effects analytically because of the harnessing of the approximation under consideration. The spacing, ds between the nano-ribbons being small, a small scale non-uniformity of the electric potential distribution in the in-plane direction y can be neglected.

In the right-hand side of eqn. (2), Σ_+ is considered to be neglected since the electron density markedly exceeds the hole density at $V_b > 0$. Considering the relationships between the electron density and the electric potential, from Eq.(2) one can arrive at the following equations governing the potential distribution in the active region:

$$\frac{\partial^2\phi}{\partial x^2} = -\frac{3}{W_b W_g}\phi = -\frac{3\left(\frac{V_b}{W_b}+\frac{V_g}{W_g}\right)}{W_b+W_g}+\frac{3V_b}{(W_b+W_g)W_b}\exp\left(\frac{e\phi}{K_BT}\right) \qquad (4)$$

$$\frac{\partial^2\phi}{\partial x^2} = -\frac{3}{W_b W_g}(\phi - V_d) = -\frac{3\left(\frac{V_b}{W_b}+\frac{V_g}{W_g}\right)}{W_b+W_g}+\frac{3V_b}{(W_b+W_g)W_b}\exp\left(\frac{e\phi-V_d}{K_BT}\right) \qquad (5)$$

If the electron gas is non-degenerate, the dependences of the exponential term in the right-hand sides of (4) and (5) are valid. The threshold value of the back gate voltage, at which the degeneration of the electron gas occurs, can be estimated as $V_b V_F$.

2.3 Potential Distributions at Low Top-Gate Voltages

Since the modulus of the potential $|\varphi|$ can be not that large when the top gate is negative ($V_g < 0$) and its absolute value $|V_g|$ is sufficiently small, (4) and (5) can be linearized and presented in the following form:

$$\frac{\partial^2\phi}{\partial x^2}-\frac{3}{W_b W_g}\left[1+\frac{W_g}{W_b+W_g}\frac{eV_b}{K_BT}\right]\phi = -\frac{3v_g}{(W_b+W_g)W_g} \qquad (6)$$

$$\frac{\partial^2\phi}{\partial x^2}-\frac{3}{W_b W_g}\left[1+\frac{W_g}{W_b+W_g}\frac{e(V_b-V_d)}{K_BT}\right]\phi = -\frac{3\left(\frac{v_g}{W_g}-\frac{V_d}{W_b}\right)}{(W_b+W_g)} \qquad (7)$$

$V_g \ll 0$. At $V_d = 0$, (6) and (7) yield

$$\phi \simeq \frac{V_g W_b}{W_b+W_g}\frac{\left[1-\frac{\cosh\left(\frac{x}{\lambda}\right)}{\cosh\left(\frac{L_g}{2\lambda}\right)}\right]}{\left[1+\frac{W_g eV_b}{(W_b+W_g)K_BT}\right]} \qquad (8)$$

where

$$\lambda - \frac{\Lambda}{\sqrt{\left(1+\frac{W_g}{W_b+W_g}\frac{eV_b}{K_BT}\right)}} = \frac{\Lambda}{\sqrt{\left(1+\frac{W_g}{W_b+W_g}\frac{eV_b}{K_BT}\right)}} \qquad (9)$$

Is the effective screening length and $\Lambda = \sqrt{(W_b W_g/3)}$. At $V_d = 0$ as follows from eqn. (6), the function exhibits a minimum $\phi = \phi_{m0}$ at x = 0 with

$$\phi_{mo} \simeq \frac{V_g W_b}{W_b+W_g}\frac{\left[1-\frac{1}{\cosh\left(\frac{L_g}{2\lambda}\right)}\right]}{\sqrt{\left(1+\frac{W_g}{W_b+W_g}\frac{eV_b}{K_BT}\right)}} \simeq \frac{V_g W_b K_B T}{V_b W_g e} \qquad (10)$$

Here, we have taken into account that normally $V_b \gg K_B T/e$ and $L_g \gg$ (with $<$).

$$\phi_m \simeq \phi_{mo} \simeq \frac{V_g W_b K_B T}{V_b W_g e} \qquad (11)$$

Comparing $e|\phi_m|$ given by eqn. (9) with K_BT, we find that (4), (5), (6), (7) and (8) are valid when $|V_g| \lesssim V_b W_g/W_b$.

2.4 Potential Distributions at High Top-Gate Voltages

At high back gate voltages, the quantity playing the role of the screening length is rather small. In this case, the length of the regions near the points $x = L_g/2$, in which the potential changes from $\phi = 0$ to $|\phi| > K_BT$ and from $\phi = V_d$ to $|0\phi V_d| > K_BT$,is small in comparison with the top gate length L_g. In such short regions near $x = \pm Lg/2$, the potential distribution can still be describe by eqn. (7). However, in a significant part of the active region the electron charge, which is in such a situation exponentially small, can be disregarded and the last (exponential) terms in (4) and (5) can be omitted.

Thus at high top gate voltages, (4) and (5) in the central region can be presented in the following form:

$$\frac{\partial^2 \phi}{\partial x^2} - \frac{3}{W_b W_g}\phi = -\frac{3\left(\frac{V_g}{W_g}+\frac{V_d}{W_b}\right)}{(W_b+W_g)} \qquad (12)$$

Solving (11) using boundary conditions given by eqn. (3), we arrive at

$$\phi = \left(V_g + \frac{V_b W_g}{W_g}\right)\left(\frac{W_b}{W_b+W_g}\right)\left[1 - \frac{\cosh\left(\frac{x}{\Lambda}\right)}{\frac{L_g}{2\Lambda}}\right] + \frac{V_d\left(\frac{\sinh\left(x+\frac{L_g}{2}\right)}{\Lambda}\right)}{\sinh\left(\frac{L_g}{\Lambda}\right)} \qquad (13)$$

At $V_d = 0$, ϕ exhibits a minimum at $x = 0$ and

$$\phi_{mo} \simeq \left(V_g + \frac{V_b W_g}{W_g}\right)\left(\frac{W_b}{W_b+W_g}\right)\left[1 - \frac{1}{\cosh\left(\frac{L_g}{2\Lambda}\right)}\right] \qquad (14)$$

At reasonable values of the drain voltage V_d (sufficiently small compared to V_b), eqn. (11) yields

$$\phi_m \simeq \left(V_g + \frac{V_b W_g}{W_g}\right)\left(\frac{W_b}{W_b+W_g}\right)\left[1 - \frac{1}{\cosh\left(\frac{L_g}{2\Lambda}\right)}\right] + \frac{V_d}{2\cosh\left(\frac{L_g}{2\Lambda}\right)} \qquad (15)$$

Fig.3 and Fig.4 show examples of the spatial distributions (along the channel, i.e., in the x direction) of the electric potential in the active region (under the top gate) calculated for a GNR FET with $W_b = 100$nm, $W_g = 30$nm , and $L_g = 300$nm at the back gate voltage $V_b = 2.0$V, assuming different values of the top gate voltage V_g and the drain voltage V_d.

As seen from Fig.3, the potential distribution markedly sags and the height of the barrier for electrons near the center increases with increasing absolute value of the top gate potential $|V_g|$.

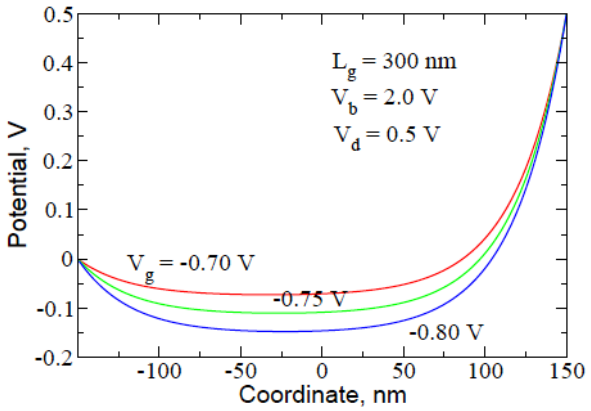

Fig.3: Spatial distributions of the potential at different top gate voltages [16]

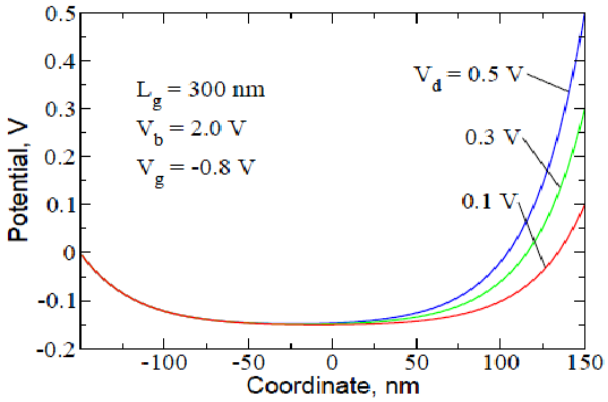

Fig.4: Spatial distributions of the potential at different drain voltages [16]

Fig.4 reveals that in the GNR-FET with chosen parameters the minimum value of the potential $ø_m$ and, hence, the height of the barrier $-eø_m$ for the electrons propagating from the source are virtually insensitive to the drain voltage. The approach used in this subsection is valid when $e|ø_m| \gg K_BT$, i.e., when $|V_g| - V_bW_g/W_b \gg K_BT(W_b+ W_g)/eW_b \sim K_BT = e$. In the limit $L_g \gg \Lambda > \lambda$ the equations for $ø_m$ obtained above [18].

III. CALCULATION AND ANALYSIS OF CURRENT-VOLTAGE CHARACTERISTICS

The source-drain current can be determined by the electrons overcoming the potential barrier under the top gate. The density of this current (per unit length)can be derived from the following formula:

$$J = \frac{2e}{\pi\hbar d}\left(\int_{P_m^p}^{\infty} vp f_p^d \, dp\right) \quad (16)$$

where,

$$v_p = \frac{\varepsilon_{p'>0}^{+}}{dP} v^2 \left(\frac{p}{\sqrt{(v^2p^2+\frac{\Delta^2}{4})}}\right) \quad (17)$$

is the velocity of the electron with momentum p in the lowest subband of the nanoribbon conduction band and P^s_m And P^d_m are the moments of the electrons with the energies $e|ø_m|$ and $e|phi_m + V_d)|$, respectively. We have taken into account that the nano-ribbon array is dense: ds ≪ d. Integrating in eqn. (16), we arrive at:

$$J = v\left(\frac{\alpha}{\frac{3}{2\pi^2}W_b}\right)\sqrt{\left(\frac{K_BT}{\Delta}\right)}\exp\left(\frac{eø_m}{K_BT}\right) \times [V_b - (V_b - V_d)\exp\left(-\frac{eV_d}{K_BT}\right)] \quad (18)$$

3.1 Current versus Drain Voltage

The dependence of the source-drain current on the drain voltage is associated with the dependence of $Ø_m$ on this volt- age given by (21) and (25) and the voltage dependence of the last factor in the right-hand side of eqn. (29). At low top gate voltages ($|V_g| \lesssim v_gW_g/W_b$), using (21) and (29), we get:

$$J \propto [V_b - (V_b - V_d)\exp\left(-\frac{eV_d}{K_BT}\right)] \quad (19)$$

i.e., $J \propto V_d$ If $V_d \lesssim K_BT/e$, and J = const. If ($K_BT/e \ll V_d < v_gW_g/W_b$). At moderate and high top gate voltages when $ø_m$ is given by eqn. (16), we arrive at the following dependence

$$J \propto \exp\left[\frac{eV_d}{2K_BT\cosh\left(\frac{L_g}{2\lambda}\right)}\right] \times [V_b - (V_b - V_d)\exp\left(-\frac{eV_d}{K_BT}\right)] \quad (20)$$

At $V_d \lesssim K_BT/e$,eqn. (21) yields the same linear dependence on the drain voltage as that described by (19). When$V_d \gg K_BT/e$, we obtain:

$$J \propto \exp\left[\frac{eV_d}{2K_BT\cosh\left(\frac{L_g}{2\lambda}\right)}\right] \quad (21)$$

3.2 Current versus Gate Voltages

According to (10), (14), and (17), the source-drain current as a function of the top gate voltage is described by the following relations:

$$J \propto \exp\left[\frac{V_gW_b}{V_bW_g}\right] \quad (22)$$

At $|V_g| \lesssim V_bW_g/W_b$.

$$J \propto \exp\left[\frac{eV_g W_b}{K_B T(W_b+W_g)}\left(1-\frac{1}{\cosh\left(\frac{L_g}{2\Lambda}\right)}\right)\right] \quad (23)$$

At $|V_g| \gtrsim V_b W_g/W_b$.

According to (22) and (23), the dependence of the source-drain current on the top gate voltage is much steeper in the range high top gate voltages $|V_g|$ &$V_b W_g/W_b$than at $|V_g| \gtrsim V_b W_g/W_b$, i.e., when the central region of the channel becomes essentially depleted. The source-drain current versus the back gate dependence at high top gate and drain voltages is given by

$$J \propto V_b \exp\left[\frac{eV_g W_b}{K_B T(W_b+W_g)}\left(1-\frac{1}{\cosh\left(\frac{L_g}{2\Lambda}\right)}\right)\right] \quad (24)$$

The source-drain current increases with increasing backgate voltage due to the pertinent increase in the electron density in all regions of the channel.

3.3 Description of Numerical Simulation

The description of all the inputs and outputs used for numerical simulation has been presented in this section. The input symbols used in the theoretical part have been described in Table 1. In Table 2, the output symbols have been listed.

Table 1: Description of the inputs of all the symbols used in the theoretical part [19]

Inputs			
Symbol	**Description**	**Unit (S.I.)**	**Variable**
L_g	Length of the top gate	nm	L_g
W_b	Thicknesses of layers between graphene and the back gate	nm	W_b
W_g	Thicknesses of layers between graphene and the top gate	nm	W_g
æ	Dielectric constant of materials between the channel and gates	F/m	ae
V_b	The back gate voltage	Volt	V_b
V_d	The potential of the drain contact	Volt	V_d
V_g	The top gate voltage	Volt	V_g
ø	The electrostatic potential	V	F_m
e	elementary charge	Coulombs	e
ψ	The electric potential	V	Psi
υ	the characteristic velocity of the electron	cm/s	V
Δ	Energy Bandgap	eV	delta
K_B	Boltzman Constant	$m^2kgs^{-2}K^{-1}$	K_B
T	Temperature	Kelvin	T

Table 2: Description of the outputs of all the symbols used in the theoretical part [19]

Outputs			
Symbol	**Description**	**Unit (S.I.)**	**Variable**
J	Current density	(mA/cm)	J
I_{on}	Current in On condition	Amber	I_{on}
I_{off}	Current in Off condition	Amber	I_{off}

IV. RESULTS AND ANALYSIS

The current density versus drain voltage dependences for GNRFET calculated for different top gate voltages V_g are shown in Fig.5. The calculation is done for L_g = 300nm at the back gate voltage V_g = 2V and Δ = 0.4 eV, æ = 4, W_b = 100 nm, W_g = 30 nm, and T = 300 K. From Fig. 5, it is seen that the source-drain current as a function of the drain voltage in a GNRFET with relatively long gate (Lg = 300nm) exhibits saturation starting rather low drain voltages. This is a consequence of very weak sensitivity of the potential barrier for the electrons propagating from the source to the drain voltage [13]. The transformation of the J vsV_d dependences with varying top gate voltage in the range of the latter $|Vg| > V_b W_g = W_b$. These indicate strong sensitivity of the source-drain current to the gate voltages.

Now considering (20) and (23), it is seen that the source-drain current saturates when V_d becomes larger that KBT=e in a GNR-FET with a long top gate, whereas in a GNRFET with L_g comparable with Λ, the source- drain current markedly increases with increasing V_d even at rather large values of the latter. This phenomenon is shown in Fig.6 (a), (b) by the calculation of current-voltage characteristics for GNRFETs with long (L_g = 300nm) and short (L_g = 100nm) top gates.

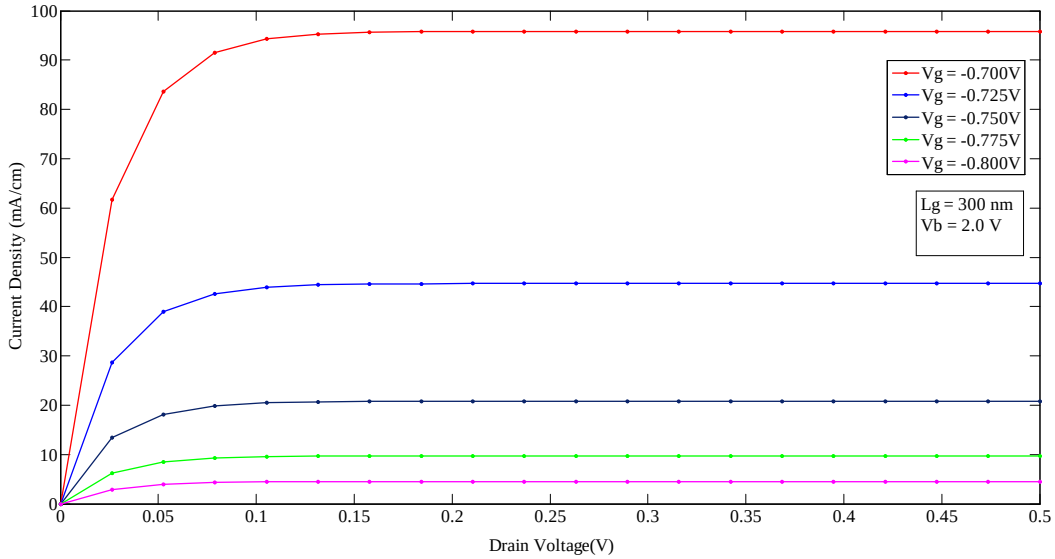

Fig.5: The source-drain current density versus drain voltage dependencies at fixed back gate voltage (V_b=2.0V) and different top gate voltages V_g.

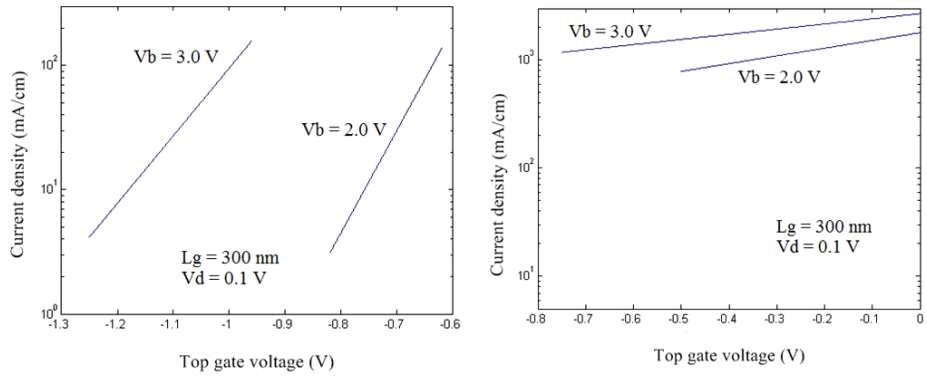

(a) (b)

Fig.6: (a), (b) The source-drain current density as a function of the top gate voltage at different back gate voltages. [19]

Now, we examine the switching behavior of GNRFET. Similar to the previous section, we assume Δ = 0.4 eV, æ = 4, W_b = 100 nm, W_g = 30 nm, and T = 300 K. For switching on and switching off condition, we have considered drain voltage V_d= 0.5V and back-gate voltage V_b= 2V. The gate voltage is varied within -0.7V to -0.8V and the switch on and switch off curve is shown in Fig.7 (a) and (b) respectively. It is seen that current density varies reciprocally under particular length for different top gate voltages for On condition. From another point of view, the current density decreases as the channel length increases for fixed value of gate-voltage. On the other hand, the switching off condition remains same for all gate voltages applied. Therefore, reducing the channel thickness can result in better performance of the device. The ratio of current in *On* condition and current in *Off* condition for different gate voltages V_g are shown in Fig.8.

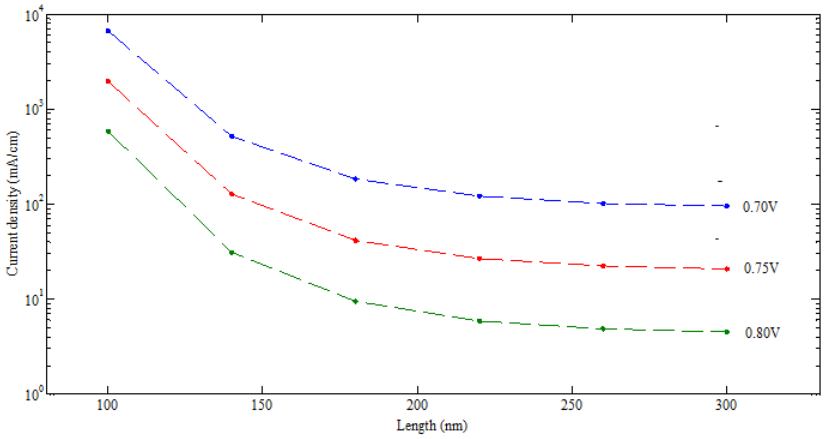

(a)

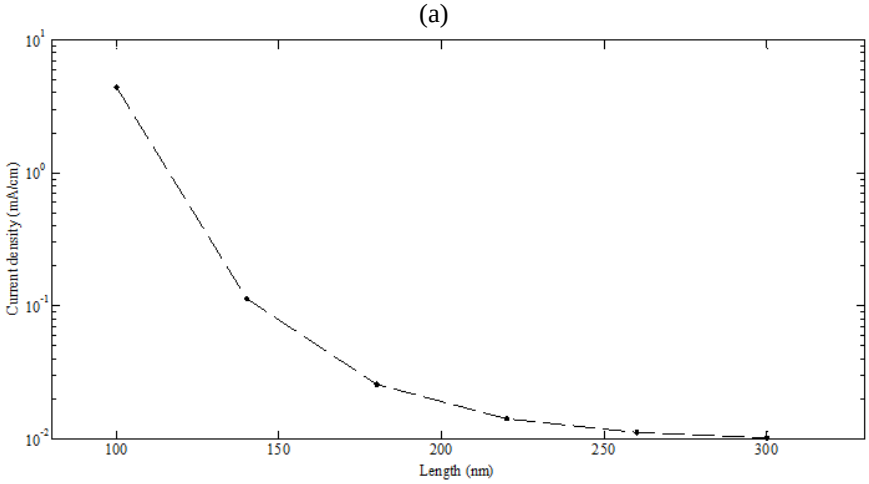

(b)

Fig.7: (a) Current in *on* condition, I_{ON};
(b) Current in *off* condition, I_{OFF}

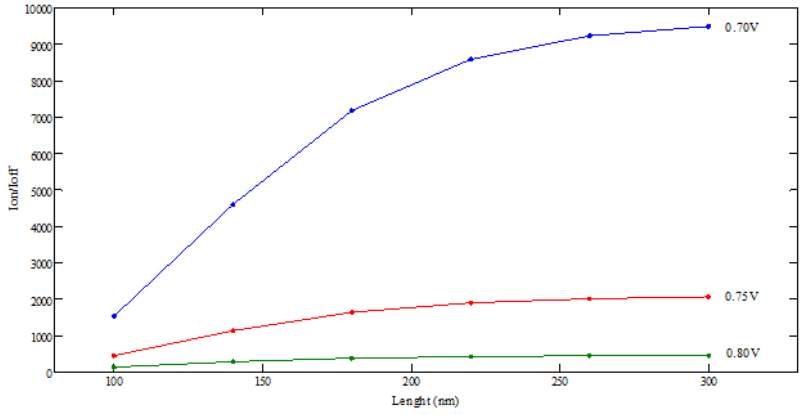

Fig.8: Ratio of I_{ON} and I_{OFF} for different gate voltages, V_g

V. CONCLUSION

In this study, we have examined the current-voltage relationship of GNRFET and the switching on and switching off properties in terms of current density, channel length and gate-voltage. Our experiment includes the dependencies of the source-drain current versus the drain voltage as well as the back gate and top gate voltages. The shortening of the top gate can result in a substantial modification of the GNRFET current-voltage characteristics. The band gap of the GNR channel strongly depends on its width, which significantly affects the on current and off current. Although our analysis has not been performed under excessively high back gate voltages due an assumption that the electron gas in the channel is non-degenerate, the results show that the analysis can be utilized for GNRFET optimization.

REFERENCES

[1] K. S. Novoselov, A. K. Geim, S. V. Morozov, D. Jiang, Y. Zhang, S. V. Dubonos, I. V. Grigorieva, and A. A. Firsov, *Science 306*, 666 (2004).

[2] A. K. Geim and K. S. Novoselov, *Nature Mater. 6*, 183 (2007).

[3] J.H. Chen, C. Jang, S. Xiao, M. Ishigami, and M. S. Fuhrer, *Nat. Nanotechnol. 3*, 206 (2008).

[4] M. C. Lemme, T. J. Echtermeyer, M. Baus, and H. Kurz, *IEEE Electron Device Lett. 28*, 282 (2007).

[5] Meric, N. Baklitskaya, P. Kim, and K. L. Shepard, Tech. Dig.,*Int. Electron Devices Meet. 2008*, 21.2.

[6] Fujita M., Wakabayashi K., Nakada K. and Kusakabe K. (1996). Peculiar Localized State at Zigzag Graphite Edge, *Journal of the Physics Society Japan 65 (7)*: 1920.

[7] Nakada K., Fujita M., Dresselhaus G. and Dresselhaus M.S. (1996). Edge state in graphene ribbons: Nanometer size effect and edge shape dependence. *Physical Review B 54 (24)*: 17954.

[8] Wakabayashi K., Fujita M., Ajiki H. and Sigrist M. (1999). Electronic and magnetic properties of nanographite ribbons. *Physical Review B 59 (12)*: 8271.

[9] M. Han, B. Zyilmaz, Y. Zhang, and P. Kim, *Phys. Rev. Lett. 98*, 206805 (2007).

[10] D. Jimnez and O. Moldovan, Explicit drain-current model of graphene field-effect transistors targeting analog and radio-frequency applications, *IEEE Trans. Electron Devices, vol. 58, no. 11, pp. 40494052*, Nov. 2011.

[11] Cresti, A.Proposal for a graphene-based current nanoswitch, *Nanotechnology, 19(26):265401*, 2008

[12] Jyotsna, C. and G. Jing, Atomistic simulation of graphene nanoribbontunneling transistors, 2010 *3rd International Nanoelectronics Conference (INEC)*, Hong Kong, January 3-8, 200-201, 2009.

[13] Liang, G.C., N. Neophytou, "Performance projections for ballistic graphene nanoribbon field-effect transistors", *IEEE Transaction on Electron Devices, 54(4):677-682*, 2007.

[14] Pei, Z., M. Chowdhury, Analytical Theory of Graphene Nanoribbon Transistors, *Proceedings of the 2008 IEEE International Workshop on Design and Test of Nano Devices, Circuits and Systems*, Cambridge, MA, September 29-30, 3-6, 2008

[15] S. A. Thiele, J. A. Schaefer, and F. Schwierz, Modeling of graphene metal-oxide-semiconductor field-effect transistors with gapless large-area graphene channels, *J. Appl. Phys., vol. 107, no. 9, pp. 094505-1094505-8*, May 2010.

[16] I. Ryzhii and I. I. Khmyrova, "Current-voltage characteristics of a graphene nanoribbon field-effect transistor", *Sov. Phys. Semicond. 22, 807* (1988).

[17] Razali Ismail, Mohammad TaghiAhmadi, Sohail Anwar, *Advanced Nanoelectronics*, CRC Press, ISBN: 13:978-1-4398-5681-9 (eBook-PDF)

[18] A. A. Sukhanov and Yu. Ya. Tkach, Sov. *Phys. Semicond. 18*, 797 (1984).

[19] Rashed, M.Z., ArdalanLotfi, *A Graphene Nano-Ribbon Field-Effect Transistor Modeling Integrated System Technology*, Thesis Dissertation, Politecnico di Torino, June 5, 2014.